

Processing of Raw GNSS Reflectometry Data From TDS-1 in a Backscattering Configuration

Lucinda S. King , *Student Member, IEEE*, Martin Unwin , Jonathan Rawlinson ,
Raffaella Guida, *Member, IEEE*, and Craig Underwood , *Member, IEEE*

Abstract—Global navigation satellite system reflectometry (GNSS-R) has found many applications in the field of Earth observation including ocean wind-speed detection, ice altimetry, soil moisture monitoring, and more. The main focus of GNSS-R research to date has been on forward-scattered reflections, but theoretical work has proposed a backscattering regime and associated new application opportunities, including marine target detection. This article discusses the methods and results of processing the U.K. TechDemoSat-1 raw data collections in a backscattering regime for the first time, with initial results from sea ice datasets presented. The research has also identified a key problem with the backscatter method—for certain geometries the power from the specular point (forward scattered) may contaminate the data. The theory behind this and a method for predicting such occurrences is also discussed.

Index Terms—GNSS reflectometry, microwave reflectometry, radar data processing, radar scattering, radar target recognition, sea ice.

I. INTRODUCTION

GLOBAL navigation satellite system reflectometry (GNSS-R), a passive bistatic L-band system using navigation satellites as transmitters of ‘signals of opportunity’ (SoOP), has achieved great success in the field of ocean wind speed sensing. Missions such as UK-DMC (launched in 2003) and TechDemoSat-1 (also U.K., launched in 2014) proved that the technique was viable on a space-borne platform and opened the door for the NASA CYGNSS mission (constellation of 8 satellites, launched in 2016), as well as providing valuable data in their own right. The data from both TechDemoSat-1 (TDS-1) and CYGNSS has been of great value to the scientific community, with a wide range of applications being explored including soil moisture and flood inundation. These applications all exploit the bistatic nature of GNSS-R which allows forward-scattered signals to be collected. In these applications, the major scattering component is specular, which favors the forward-scattering geometry.

Manuscript received December 5, 2019; revised March 2, 2020, April 13, 2020, and May 11, 2020; accepted May 19, 2020. Date of publication May 28, 2020; date of current version June 16, 2020. The work of L. King was supported by a NERC SCENARIO studentship. She also received financial and technical support through partnership with Surrey Satellite Technology Ltd. (*Corresponding author: Lucinda King.*)

Lucinda S. King, Raffaella Guida, and Craig Underwood are with the Surrey Space Centre, University of Surrey, Guildford GU2 7HX, U.K. (e-mail: l.s.king@surrey.ac.uk; r.guida@surrey.ac.uk; c.underwood@surrey.ac.uk).

Martin Unwin and Jonathan Rawlinson are with the Surrey Satellite Technology Ltd., Guildford GU2 7YE, U.K. (e-mail: M.unwin@sstl.co.uk; J.rawlinson@sstl.co.uk).

Digital Object Identifier 10.1109/JSTARS.2020.2997199

Recent studies have investigated the theoretical use of GNSS-R in a backscattering geometry and the potential new applications this offers, including marine target detection [1]–[5]. At L-band the majority of the ocean-reflected radiation (termed ‘clutter’ when the aim is to detect something other than the ocean itself) is specularly scattered away from the incidence direction, i.e., forward-scattered. This means that in a backscattering geometry, the majority of the clutter will be directed away from the receiver. In contrast, a target such as a ship provides multiple bounce opportunities which increases the backscattering cross section (BCS) significantly. These include double-bounces from the ship’s hull and the sea surface, and multiple-bounces from other parts of the ship’s structure and/or the sea. A backscattering geometry is therefore predicted to have better power returns for target detection than the conventional forward-scattering mode.

This article discusses the methods and results of processing the U.K.’s TDS-1 raw data collections in a backscattering regime for the first time. The unprocessed nature of the data allows the cross-correlation process between the reflected signal and a clean copy of the transmitted signal to be targeted at delays and Dopplers from nonspecular directions. This is in contrast with the processed Level 1B delay-Doppler maps (DDMs) which have been made available by Surrey Satellite Technology Ltd. (SSTL) through the MERRByS online data service [6]. These DDMs have previously been used to investigate backscattered signals [4], however these studies were constrained to delay-Doppler space around the specular point (SP). The raw data contains signals from multiple GNSS constellations, but primarily from the global positioning system (GPS). It should be noted that the current study has only considered the GPS coarse acquisition (C/A) signals but work is ongoing on processing Galileo reflections from the raw data, both in forward and backscattering modes.

II. APPLICATIONS

A. Target Detection (Ships and Oil Rigs)

For the detection of targets such as ships the return from the ocean itself is termed ‘clutter.’ The backscattering mode of GNSS-R (bGNSS-R) offers the possibility of detecting targets over the ocean as they will present strong BCSs (σ_B) relative to the ocean clutter and should therefore show up clearly in reflected data. This is providing that they also overcome the thermal noise which is not reduced in the same way as the clutter.

The large BCS of ships is due to di- or trihedrals either present in the target itself or formed by the hull and the water, and the reflective properties of metal at L-band, the frequency of GNSS. In previous studies the target response as a whole has been modeled as a trihedral square corner reflector, with the following equation [2], [7]:

$$\sigma(x_S, y_S) = \frac{12\pi l^4}{\lambda^2} \quad (1)$$

where λ is the wavelength of the L-band carrier (approximately 19 cm) and the subscript S refers to the “ship” target. l is the interior edge size of the reflector, taken to be the dimension of the ship perpendicular to the plane of incidence. The aspect angle is therefore key to the predicted capability for detection, as reported in [2]. The same article also discusses the importance of polarization on target detection, and summarizes that ships above 20 m in size have the theoretical capability of being detected. Due to the multiple bounces, RHCP rather than the conventional LHCP is predicted to be better suited to reception of backscattered signals. In the current study, we are constrained to using LHCP-received signals due to the limitations of the hardware used. In light of this, and considering the lack of open-source historic ship location data other marine targets have been considered for study using this data—specifically oil rigs. The location of fixed oil platforms is known, meaning that results are easier to verify, and they have been shown to have high BCS in the microwave bands, and have specifically been shown to backscatter GNSS signals [4].

B. Ice Edge Detection

Monitoring changes in the location, size, and nature, etc., of ice-sheets and icebergs is of great importance for climate change monitoring and environmental science in general. Additionally, phenomena such as the widening of the North West passage are of great interest to the shipping, offshore energy and increasingly, tourism, industries.

The edge of an ice-sheet or iceberg can form a near 90° angle with the water, creating a favorable geometry for double-bounce scattering. Multiple-bounce scattering may also be possible in ice crevasses or between icebergs. In addition, the ice roughness plays a part. Ice surface roughness is dependent on the age of the ice, with young ice being smoother as it has been subject to less weathering. The dielectric constant of the ice, which varies with salinity and trapped air, and therefore age, also affects the scattering properties but this has not been taken into account in this study as to a first approximation it is not considered to limit the direction of scattering in the same way as geometry.

In general, reflections from ice will be a combination of specular and diffuse. Both cases can result in radiation being backscattered to the receiver: a single instance of diffuse scattering from rough ice could have this result, as would multiple-bounce specular scattering from smooth ice. As the power will be less spread out in the latter case, stronger returns are expected in this scenario, and therefore this method will be used to target ice edges. In addition to ice edges and the sea surface, missing chunks, crevasses or other structures in the ice may create natural

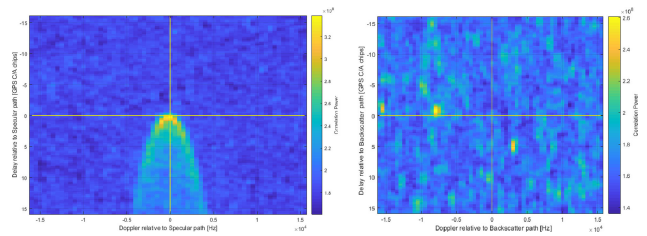


Fig. 1. (Left) Typical forward-scattered DDM from an ocean GPS reflection. (Right) Example of a bDDM from the Antarctic region, showing three features of high signal power with respect to the background which may be indicative of sea ice (from the July 24, 2016 dataset—see also Fig. 9).

trihedral corners which could backscatter the signal, irrespective of incidence angle if the surface is smooth enough.

III. METHOD

During the period of operations of the U.K.’s TDS-1 over 200 raw data collections were made over a variety of Earth surfaces, mostly containing approximately 2 min. of data. This was in addition to the DDMs which were generated on board and disseminated via the MERRByS data service. These raw data are the unprocessed recordings from the instrument front end and offer opportunities for new modes of processing other than those used on board. For this research a software-defined receiver which had previously been used to process raw data for forward scattering was updated to predict backscatter reflection points (BRPs).

For forward scatter, the form of the reflected signal as seen in the DDM is generally well understood. A characteristic forward scatter DDM over the ocean shows a strong peak reflection corresponding to the SP, and “arms” which represent the scattering from the glistening zone (GZ), as shown in Fig. 1. The arms appear weaker for stronger coherent reflections and sometimes disappear completely.

For backscatter, the expected form of the DDM is different. A return from a backscattering target should show up as a strong peak in the backscattered DDM (bDDM), however not necessarily at the centre—which corresponds to the delay-Doppler of the BRP. Depending on the location and orientation of targets, backscattered reflections may be possible from points away from the specifically derived BRP (analogous to forward-scattered returns coming from the whole GZ). There will therefore be no characteristic parabola shape, rather individual bright “features” against a background of clutter. These bright features may cover several pixels due to the point spread function and this can be used to distinguish targets from individual noise pixels [4].

It should be noted that the backscatter DDM can be visualized as a subsection of an extended forward-scatter DDM, as can be understood from Figs. 2 and 9. The orientation of the delay and Doppler lines depends on the orientation of the incidence plane (the plane containing transmitter, receiver, and reflection point) and the direction of motion of the receiver. The orientation of the Doppler lines relative to the backscatter point is particularly important, as it determines the size and shape of the pixels surrounding the backscatter point. In certain scenarios, the delay

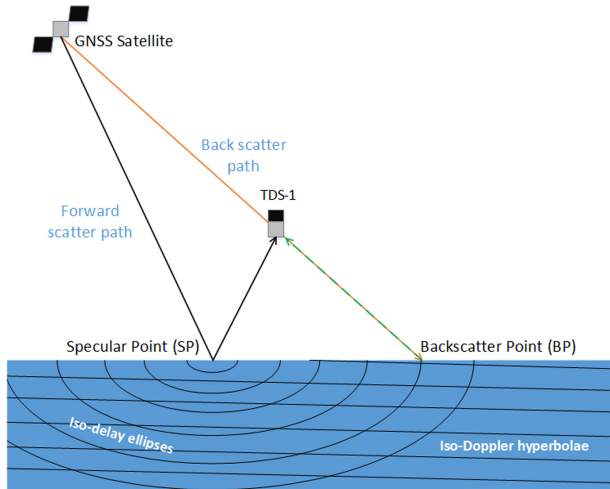


Fig. 2. Geometry of GNSS-R backscatter—note that the iso-delay and iso-Doppler lines correspond to just one possible instance of this geometry, and will change with, e.g., the direction of motion of the receiver relative to the incidence plane.

and Doppler lines at the backscatter point may be almost aligned (see the bottom of Fig. 2), resulting in very elongated pixels, which are less suitable for target detection.

One final point of interest regarding the bDDMs is that due to geometry the BRP lies at the intersection of the Earth ellipsoid and the incidence plane, and therefore will always lie on the semimajor axis of the iso-delay ellipses surrounding the SP. This can assist with checking the accuracy of the prediction of the backscatter point.

A. Backscatter Point Prediction

The GNSS-R software receiver used, developed alongside the SGR-ReSI reflectometry payload [8] which flew on TDS-1, works in the conventional (forward-scatter) sense by predicting an SP using the positions of transmitter and receiver and a quasi-spherical Earth model, then using this position and relative velocities to generate the predicted delay and Doppler of a signal reflected from that point. A clean replica for correlation is then generated on board with these values of delay and Doppler.

In order to update this tool for a backscattering configuration, it was necessary to predict backscatter points (BRP). Figs. 2 and 3 show the geometry of such a configuration in which the BRP is defined the point at which the line passing through the transmitter and receiver intersects the Earth's surface. For the purposes of this research, the Earth's surface has been taken to be the WGS84 ellipsoid with equation

$$\frac{x^2}{a^2} + \frac{y^2}{a^2} + \frac{z^2}{b^2} - 1 = 0 \quad (2)$$

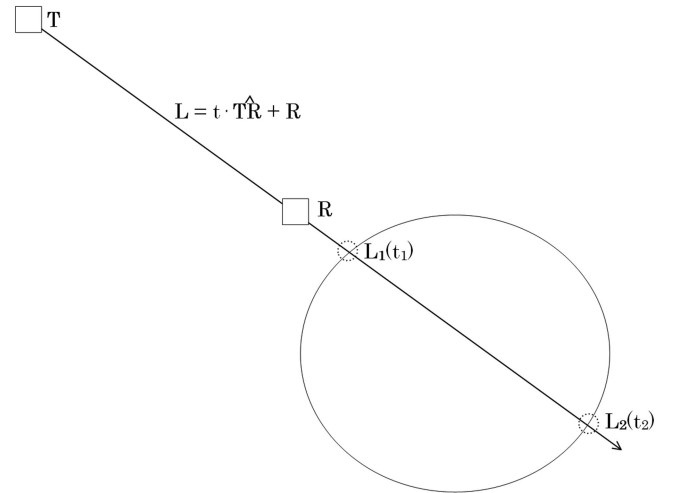


Fig. 3. Predicting the backscatter point using the intersection of a parameterised line and an ellipsoid (shown in 2-D here and not to scale).

where a and b are the Earth's WGS84 equatorial and polar radii, respectively, as defined in [9].

To predict the BRP, the transmitter and receiver positions (\mathbf{T} and \mathbf{R}) in the Earth-centred-Earth-fixed frame (ECEF) are used to form a parameterized line equation in parameter t

$$\hat{\mathbf{T}}\mathbf{R} = \frac{\mathbf{R} - \mathbf{T}}{|\mathbf{R} - \mathbf{T}|} = (u, v, w) \quad (3)$$

$$\mathbf{L} = \mathbf{R} + t \cdot \hat{\mathbf{T}}\mathbf{R} = (x + tu, y + tv, z + tw) \quad (4)$$

where $\hat{\mathbf{T}}\mathbf{R}$ is the transmitter-to-receiver unit vector, \mathbf{L} is a dummy variable representing a point lying on the line defined by the parameterized line equation, and x, y, z, u, v, w are the individual components of the three-dimensional (3-D) vectors labeled to ease the equation manipulation. Fig. 3 also gives a description of these variables.

To find the point(s) of intersection of the line (representing the signal) and the ellipsoid, (4) is substituted into (2) and expanded. The resulting quadratic equation is then solved for the line parameter, t , which can be substituted into (4) to give the location of the reflection point in ECEF. There will be two solutions for t , one for the line entering and one for it leaving the Earth. The smaller of the two should be selected, resulting in (5) for t , as shown at the bottom of this page.

The authors would like to note that a similar concept was arrived at independently by Southwell and Dempster, as described in [10].

There will be some discrepancy between the predicted point and the actual reflection point from the Earth's surface. The effect of topography on the prediction of both forward and

$$t = \frac{-1}{b^2(u^2 + v^2) + a^2w^2} \cdot \left\{ b^2(xu + yv) + a^2zw + \sqrt{[b^2(xu + yv) + a^2zw]^2 - [b^2(u^2 + v^2) + a^2w^2][b^2(x^2 + y^2 - a^2) + a^2z^2]} \right\} \quad (5)$$

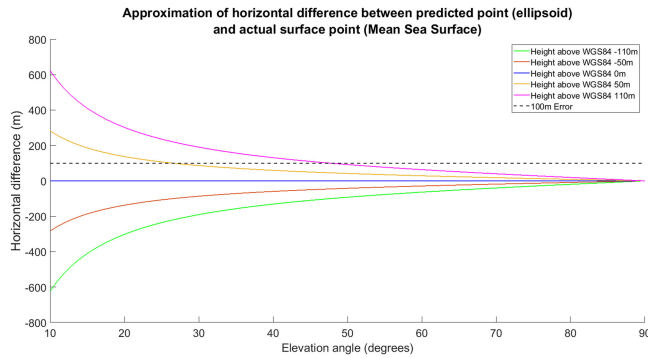


Fig. 4. Approximation of horizontal error in reflection point prediction caused by deviation of actual sea surface from the reference WGS84 ellipsoid. Calculated using $\text{horzError} = \Delta h / \tan(\text{elevation})$.

backscatter points is nontrivial and some assumptions have been made in this regard.

- 1) As discussed, the WGS84 ellipsoid has been used as an approximation to the surface. Errors relating to this approximation over the ocean are considered negligible for this initial research due to the following: over the ocean, the surface is approximated by the mean sea surface (MSS). This is a combination of the geoid and long term dynamic effects described by Dynamic Ocean Topography—the difference between the geoid and MSS is up to 2.5 m [11]. In turn, the maximum departure of the geoid from the reference ellipsoid is 105 m [12], meaning over the ocean there is an approximate maximum error of 107.5 m. Approximating the ellipsoid with a local plane, the maximum horizontal error for all elevation angles above 10° is ~ 600 m, as shown in Fig. 4. For elevation angles above 50° , which is the case for the scenarios under test, the error is around 100 m. The spatial resolution of DDM pixels is at best, i.e., under coherent scattering conditions, limited to the first Fresnel zone [13]. For the GPS L1 frequency used here (1.57542 GHz) the first Fresnel zone is of the order of 500 m and the spatial resolution will worsen in diffuse scattering conditions such as over the ocean, and thus will always be worse than the potential errors from this approximation. At this proof of concept stage, this level of accuracy is sufficient for assigning strong backscattered power returns to a surface location.
- 2) Over the land topography results in more dramatic departures of the surface from the ellipsoid. Digital elevation maps can be used to assist more accurate prediction of the reflection points however as the current study does not consider land reflections this is not considered further here.
- 3) The Earth’s rotational motion is also not taken into account. The maximum possible surface motion is ~ 30 m, calculated using the time taken for a signal to travel from Medium Earth orbit to the fastest moving point of the surface—a point at the equator.

It should be noted that the existence of BRP is not guaranteed—certain geometries could result in the line not intersecting the Earth’s surface; such cases result in complex

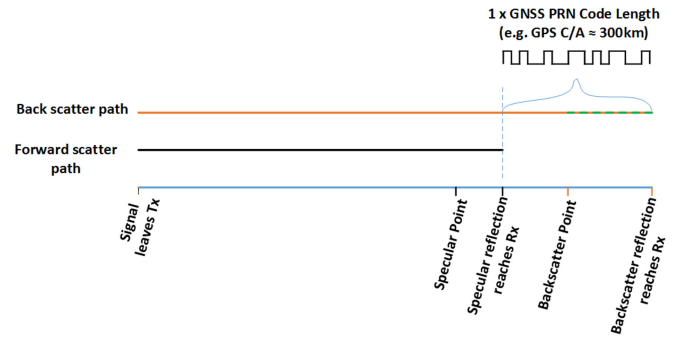


Fig. 5. GNSS code wrap-around. Tx = Transmitter, Rx = Receiver.

values for the line parameter t and are rejected. The BRP is also used in the software receiver to predict the antenna gain of TDS-1 in the direction of the reflection. This is used to reject reflections below a 0 dB gain threshold.

B. Specular Point Power Intrusions

For any receiver/transmitter pair that generates a valid BRP, a SP can also be defined. The bistatic nature of GNSS-R means that signals can be collected from forward and backscattering directions, and the majority of the power return will be from the SP due to Fermat’s principle of least action [14]. In many cases, this will not be a problem for the bDDMs as the specularly reflected signal will not have the same delay-Doppler characteristics as the reflection from the BRP, and thus will be uncorrelated. However, the open-service GNSS pseudorandom noise (PRN) spreading codes repeat on short scales (e.g., the GPS C/A code has a length of 300 km) meaning there is a possibility of code wrap-around and thus “specular intrusions” to the bDDM (Fig. 5). If the path difference between the two reflection points (ΔPath) is an integer number of GNSS code lengths (L_{GPScode}), then the clean replica generated to correlate with the predicted backscatter reflection will also match the delay properties of the SP. This will result in the power at the SP being selected by the correlation process and appearing in the bDDM at delay offset zero relative to the BRP, i.e., on the Doppler axis of the bDDM. In general, a specular intrusion will appear at a delay offset d from the BRP delay where $\text{modulo}(\Delta\text{Path}, L_{\text{GPScode}}) = d$, as long as d is within the axes of the bDDM (normally ± 15 chips). For a specular intrusion to occur, the SP reflection must also have the same Doppler offset as the BRP, which is more straightforward to predict and verify. Fig. 6 gives a graphical description of the algorithm.

A bDDM with a particularly bright feature was investigated for the possibility of an intrusion. Table I contains a subset of the analysis data which demonstrates that this was the case. The path length difference between the specular and backscatter points for all time-steps was calculated and divided by the code length. The time-step with result closest to an integer (i.e., the path difference was an integer number, in this case one, of code lengths) is shown in bold-italic font. The bDDM for this time-step is shown in Fig. 7, where it can be seen that the bright feature is nearly aligned on the zero-delay axis. In this case

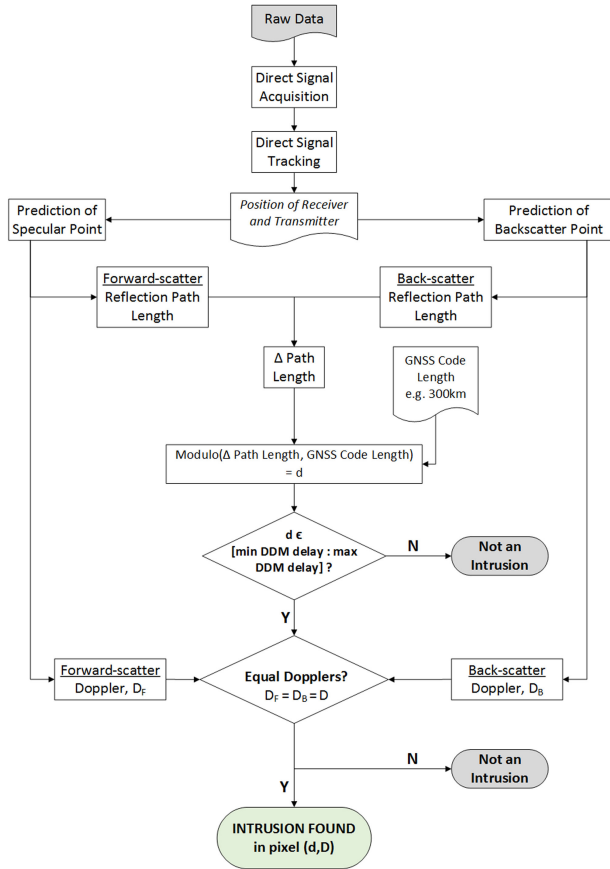


Fig. 6. Intrusion checker algorithm. This process is repeated at every measurement time step and for every tracking channel, which will each be tracking a different satellite transmitter.

TABLE I
PATH LENGTH DATA DEMONSTRATING CODE WRAP-AROUND
 $L_{code} = 299792.458$ m

Time Step (GPS seconds)	Specular Point Reflection Range (RSP, m)	Backscatter Point Reflection Range (RBP, m)	F = (RBP - RSP) / L_{code}	1 - F
469948.1	21133961.71	21434495.03	1.002471	0.002471
469948.6	21133593.68	21433873.82	1.001627	0.001627
469949.1	21133223.30	21433249.41	1.000779	0.000779
469949.6	21132868.48	21432649.39	0.999961	0.000039
469950.1	21132503.17	21432033.76	0.999126	0.000874
469950.6	21132151.56	21431439.55	0.998317	0.001683
469951.1	21131792.81	21430834.72	0.997496	0.002504

The **bold-italic** text indicates the time-step in which the specular intrusion was found on the zero-delay axis.

$\text{modulo}(\Delta\text{Path}, L_{\text{GPScode}}) \approx 0$. The predicted Doppler for the SP and backscatter point reflections was compared and found to be the same.

If bGNSS-R is to be developed as a method, especially looking to the future and potentially automated target detection, such intrusions will have to be predicted and removed in order to prevent false positives. A software tool has been developed to assist the receiver in automatically detecting bDDMs containing

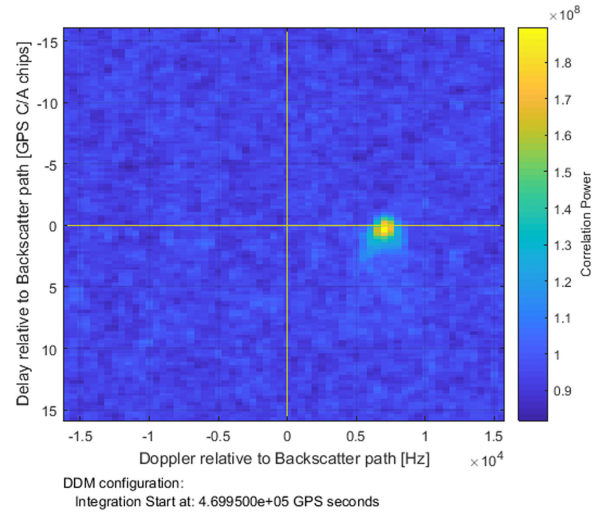


Fig. 7. bDDM at time-step 469 950 GPS seconds, showing the specular intrusion crossing the zero-delay axis. At this time-step the path-difference between the SP and BP was exactly one code length (within acceptable error).

intrusions and raising a flag, as well as providing the affected time-steps and delay-Doppler pixel(s) to enable rapid inspection.

Testing the tool on the dataset previously discussed, the outputs demonstrate that the specular intrusion moves through the bDDM from top to bottom (-15 to $+15$ delay chips) over 36 time-steps, which is borne out by the generated bDDMs. After this validation, the intrusion checker was run on the raw data collections. Each raw data collection contains reflections from more than one GNSS transmitter, identified by their PRN number. So far 125 raw datasets have been analyzed using the intrusion checker, which contain backscatter reflections from approximately 226 GPS satellites. The tool predicts specular intrusions for 41 satellites, from 34 datasets—18% of transmitting satellites result in a specular intrusion. However for some of the satellites predicted to have specular intrusions, the BRP is rejected by the antenna gain threshold and so bDDMs are not produced, and there is nothing to contaminate. Of all the specular intrusions predicted, six are for satellites not rejected. Therefore on average 2.7% of produced bDDMs will contain a specular intrusion under the current spacecraft and simulation parameters.

IV. BACKSCATTERING GNSS-R RESULTS

A large set of raw data collections were made using TDS-1 from December 2015 to March 2019. These data collections were sorted by the location of the subsatellite track to form a coarse estimate of surface type and then a down-selection was made in order to investigate the use cases described in Section II. Once bDDMs had been generated they were manually inspected for the presence of strong power returns.

A. Oil Rigs, Gulf of Mexico

Proving the concept of bGNSS-R for detection of ships is difficult due to the spatial resolution and the lack of ground

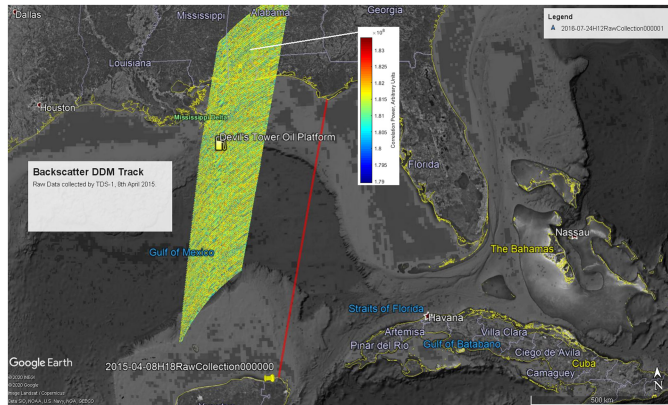


Fig. 8. Section of the Gulf of Mexico containing the Devil's Tower surface oil rig installation and overlaid with spatially mapped backscatter DDMs. The bDDM color scale represents uncalibrated power counts, the colorbar shown is representative of the track.

truth data for the historical location of ships. Oil rigs have previously been suggested as alternative, fixed targets, which should have high BCS as they are large, predominantly metallic structures [4].

This theory has been tested using raw GNSS-R data. The Gulf of Mexico was selected for this analysis due to the prevalence of oil rigs in the area and a number of backscatter point reflection tracks passing over the region. Fig. 8 shows the backscatter track considered, from the April 8, 2015 dataset, using the standard 1 ms coherent integration time.

As shown by the figure, the DDMs generated from this dataset do not contain any significant backscattered features—that is, pixels with power significantly higher than the clutter, even when crossing the oil rig directly. This can be compared with Fig. 9 where the bDDMs containing backscatter features can be clearly seen. One possible explanation for this is that dihedral scattering may be the predominant scattering mechanism from the oil rig, resulting in RHCP returns. This would explain why the backscattered power is not detected by TDS-1, and it also seems to confirm the findings of [2], which suggest that RHCP is the preferred receive antenna polarization for GNSS-R target detection.

As in general backscatter returns from targets will be coherent over a longer time than the return from the ocean surface, using longer coherent integration times may allow target signals in LHCP to rise above the clutter. However testing this using a coherent integration time of 4 ms in this dataset did not show any improvement.

B. Ice Edges, Antarctica

The possibility of using bGNSS-R for sea ice detection has also been investigated. A dataset from July 24, 2016 was chosen as the BRP track crossed a sea-ice boundary in the Antarctic, south of Argentina. Three pixels of increased signal power compared with the rest of the DDM (hereafter referred to as “features”) were found in this example, as shown in Fig. 1 (right panel) and Fig. 9. These features occurred in six consecutive DDMs (a period of 6 s), moved consistently and smoothly in

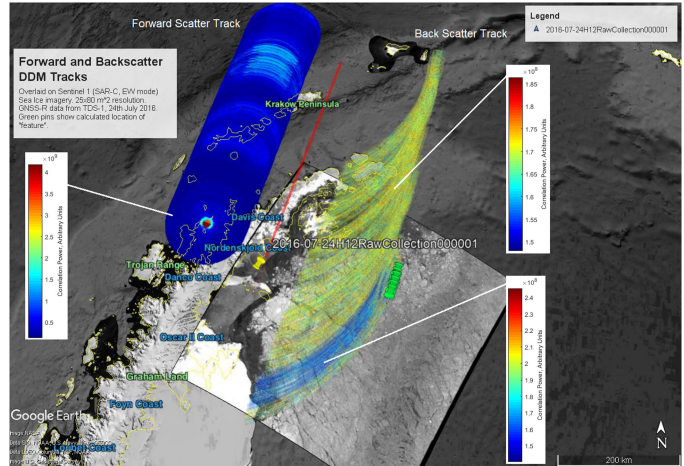


Fig. 9. Raw data collected by TDS-1, July 24, 2016 showing (from left to right) the forward scattered DDMs, the TDS-1 subsatellite track and the bDDMs mapped onto the surface. The GNSS-R data is overlaid on a Sentinel-1 image showing sea ice data at the time of the collection [15]. The blue backscatter DDMs toward the South of the track show the presence of backscattering power returns in those regions—one of these blue DDMs can be seen in a nonprojected representation in the right panel of Fig. 1. The colorbars are representative of the separate regions of the tracks indicated, a universal colorbar could not be used due to saturation.

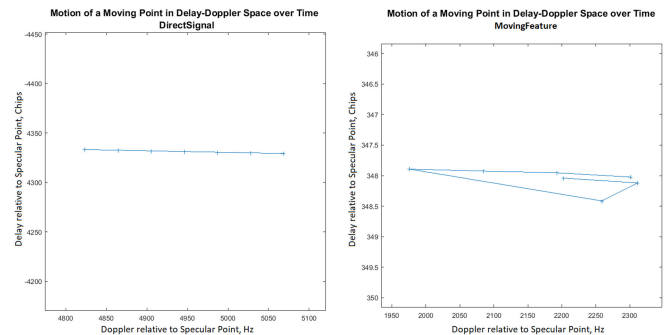


Fig. 10. Graphs showing the motion of the direct signal (left) and the strong feature (right) in delay-Doppler space relative to the SP. The characteristics of the motion are different which shows that the features are not caused by direct signal leakage.

delay-Doppler space over this time, and were fixed in delay-Doppler space relative to each other.

Sea ice maps (Figs. 9 and 12) for the date in question show there is sea ice present, and as discussed in Section II-B sea ice cliffs and crevasses are candidates for high backscatter returns. It has been proven using the intrusion checker tool that the features are not SP power intrusions, and they are not leakage of the direct signal as shown by Fig. 10. We therefore now derive a theoretical model for a structure in the ice.

As discussed in Section II-B, ice edge detection using backscattering GNSS-R can be separated into three cases based on geometry—that of coherent dihedral and trihedral reflections, and single-bounce diffuse scattering from rough ice. The case chosen for analysis in this article is the trihedral case. Although dihedral reflections from an ice edge and the ocean could produce very strong backscattered signals, they will produce

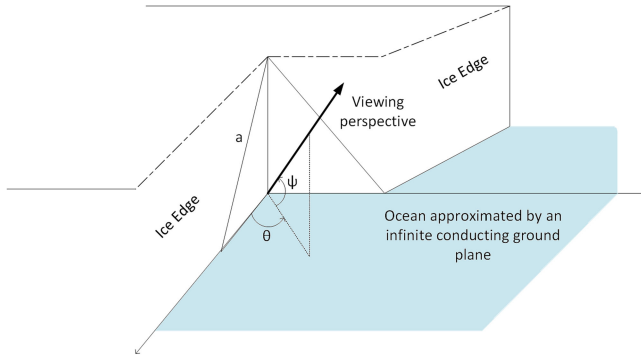


Fig. 11. Trihedral corner reflector formed by an ice edge.

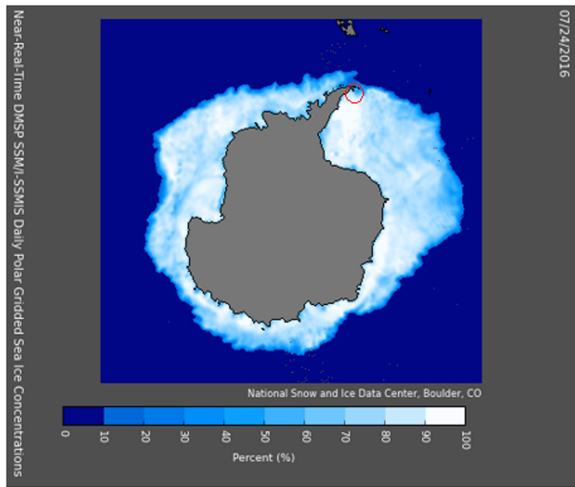


Fig. 12. Sea ice concentration map, Antarctica, July 24, 2016 [19]. Approximate location of the data collection shown by the circle.

predominantly RHCP returns and thus will largely be rejected by the TDS-1 nadir antenna. This means they are less likely to be responsible for strong GNSS-R backscatter returns. They also place a stricter requirement on the angle of the incidence plane to the target than the trihedral reflection case.

In the trihedral case, two faces of an ice edge at approximately 90° to each other and the ocean approximate a trihedral corner reflector, this could, for example, be the case after an iceberg has calved off the edge of an ice shelf. A model for the radar cross section (RCS) for such a reflector with an infinite ground plane—the ocean in this case—is given by [16]

$$\sigma(\psi, \theta) = \frac{16\pi a^4}{\lambda^2} (A_{\text{tri}})^2 \quad (6)$$

where

$$A_{\text{tri}} = \begin{cases} \sin\theta \cos\psi & \text{if } (\cos\theta - \sin\theta \geq \tan\psi) \\ \cos\theta \cos\psi & \text{if } (\sin\theta - \cos\theta \geq \tan\psi) \\ \frac{2 \sin\theta \cos\theta \cos\psi}{(\sin\theta + \cos\theta + \tan\psi)} & \text{otherwise} \end{cases}$$

and a is the edge of the triangular sections of the trihedral and λ is the carrier frequency of the incident radiation. The viewing angles ψ and θ are defined in Fig. 11. It is acknowledged that

this model for the RCS is purely geometrical, as it was derived based on the assumption of perfectly conducting faces of the trihedral. Sea water is close to a perfect conductor at GPS frequencies [17] but the two ice faces will have both roughness and dielectric properties which are not accounted for in this model, however it is still considered valid for the purposes of predicting whether backscattered power would be expected to appear above ocean clutter in this scenario. In addition, the ice faces will not necessarily be triangles and are likely to present a larger effective retroreflecting area than that assumed here, meaning this is an under-estimation of reflecting power from a geometrical perspective. Using example values of the following:

- 1) viewing angle azimuth, $\theta = 45^\circ$;
- 2) viewing angle elevation, $\psi = 65^\circ$;
- 3) trihedral side approximated by $\sqrt{2} * h_{\text{ice}}$, with $h_{\text{ice}} = 200$ m.

The RCS is calculated to be approximately 100 dB for these dimensions.

This RCS can be inserted into a bistatic radar equation (BRE) to predict the reflected power from the ice edge in such a scenario. Although the reflections will be largely coherent, the dependency on distance in the BRE will not follow the form of the coherent term in the Zavorotny–Voronovich BRE for reflectometry, updated in [18], which is proportional to R^{-2} . This is because in this scenario we are considering reflections from a finite target rather than extended plane and thus the reflector will not act like a mirror and the dependency will be on $R_1^{-2} R_2^{-2}$. The full equation is the following:

$$P_R = \frac{T_{\text{Coh}}^2 \lambda^2 P_T G_T(\mathbf{r}_t) G_R(\mathbf{r}_t) \sigma(\mathbf{r}_t) \chi^2(t - t'(\mathbf{r}_t), f - f'(\mathbf{r}_t))}{4\pi^3 |(\mathbf{R} - \mathbf{r}_t)|^2 |(\mathbf{T} - \mathbf{r}_t)|^2} \quad (7)$$

where \mathbf{r}_t is the location of the target; $P_{R,T}$ are the reflected and transmitted powers, respectively; T_{Coh} is the coherent integration time; $G_{R,T}(\mathbf{r}_t)$ are the receiver and transmitter gains toward the target location; $\sigma(\mathbf{r}_t)$ is the RCS given by (6); χ^2 is the Woodward Ambiguity Function; and \mathbf{R}, \mathbf{T} are the receiver and transmitter locations.

This equation can be used in future work to predict the backscatter returns from finite targets. At this stage a model for the RCS of the clutter has not been developed and so the powers cannot be predicted numerically, however an empirical approach has been used to predict the signal-to-noise ratio (SNR) of the backscatter power features. DDMs which do not contain the features have been averaged to form an estimate of the noise, in this case the clutter from the surface plus the thermal noise associated with the instrument. This was used to calculate an approximate SNR for the features, of -3 dB. This indicates that the apparent signal is lower than the noise, and significantly lower than would be expected if the RCS was 100 dB. A geolocation analysis carried out on the brightest feature (in the middle of the three) which mapped the pixels of the bDDM onto the surface found that over the 6 s the calculated spatial location of the feature did in fact appear to move, contrary to initial assessment, with approximately the speed of the receiver

($\sim 7.8 \text{ km s}^{-1}$) but not consistently. However, analysis has shown that the features are not due to direct signal leakage (Fig. 10).

The feature appearing to move with such speed would seem to imply that it is not a surface feature, however analysis has shown that it is also not a known instrument effect. One possible explanation is that the distortion of the delay-Doppler cells at locations far from the SP caused by the backscatter geometry gives the impression of movement. As there has not been significant research into the nature of bDDMs and this distorting affect this area is highlighted for further investigation to ensure that the observables are suitable for target detection. Another geophysical explanation is that the reflecting area contains an extended dihedral (for example, an ice cliff) and the reflection point moves across the feature with the speed of the receiver. This would also account for the reduced power on account of the mismatch in polarization with the nadir antenna, as discussed above.

V. CONCLUSION AND FUTURE WORK

This article builds on existing theoretical work and analysis using preprocessed DDMs for backscattering GNSS-R, and shows that careful considerations in processing must be made if this mode is to be pursued as an operational method. This research has shown that GNSS-R in a backscattering configuration may provide useful data in a range of scenarios, particularly when plotted onto the surface but that refinement of the processing is required. In particular the geometry of the mode and the effect on delay-Doppler space is highlighted for future research.

Scenarios analyzed in this work include sea ice detection, and a theoretical model for this is presented along with comparison with a TDS-1 raw dataset. Analysis of oil rig datasets does not show any detections using bGNSS-R, which may be due to RHCP being the preferable polarization for detecting marine targets, which is in agreement with previous literature.

Specular intrusions have been shown to be a key source of contamination in bDDMs, and a method and tool for predicting them has been presented. At this stage DDMs containing intrusions must simply be discarded; however future work could develop the tool further to remove the intrusion power using information from the forward scattered DDM. Moving forward, new signals from Galileo may be beneficial for specular intrusion mitigation thanks to longer ranging codes which will repeat less frequently.

ACKNOWLEDGMENT

The authors would like to thank the anonymous reviewers for their insightful comments which helped to improve this article. L. King would like to thank Surrey Satellite Technology Ltd., Guildford, U.K., for providing the raw TDS-1 data used in this research.

REFERENCES

- [1] M. Clarizia, P. Braca, C. S. Ruf, and P. Willett, "Target detection using GPS signals of opportunity," in *Proc. 18th Int. Conf. Inf. Fusion*, Jul. 2015, pp. 1429–1436.
- [2] A. Di Simone *et al.*, "Spaceborne GNSS-reflectometry for ship-detection applications: Impact of acquisition geometry and polarization," in *Proc. IEEE Int. Geosci. Remote Sens. Symp.*, Jul. 2018, pp. 1071–1074.

- [3] S. L. Ullo, G. Giangregorio, M. di Bisceglie, C. Galdi, M. P. Clarizia, and P. Addabbo, "Analysis of GPS signals backscattered from a target on the sea surface," in *Proc. IEEE Int. Geosci. Remote Sens. Symp.*, Jul. 2017, pp. 2062–2065.
- [4] A. Di Simone, H. Park, D. Riccio, and A. Camps, "Sea target detection using spaceborne GNSS-R delay-doppler maps: Theory and experimental proof of concept using TDS-1 data," *IEEE J. Sel. Topics Appl. Earth Observ. Remote Sens.*, vol. 10, no. 9, pp. 4237–4255, May 2017.
- [5] M. Di Bisceglie *et al.*, "Two-scale model for the evaluation of sea-surface scattering in GNSS-R ship-detection applications," in *Proc. IEEE Int. Geosci. Remote Sens. Symp.*, Jul. 2018, pp. 3181–3184.
- [6] *Measurement of Earth Reflected Radio-Navigation Signals by Satellite (MERRBYS)*, SSTL and NOC, Guildford, U.K. Accessed: Jun. 6, 2020. [Online]. Available: <http://merrbys.co.uk/>
- [7] A. W. Doerry, "Reflectors for SAR performance testing," Sandia National Laboratories, Livermore, CA, USA, Tech. Rep. SAND2008-0396, Jan. 2008. [Online]. Available: <https://www.osti.gov/biblio/929123>. Accessed on: Jun. 6, 2020.
- [8] R. de Vos van Steenwijk, M. Unwin, and P. Jales, "Introducing the SGR-ReSI: A next generation spaceborne GNSS receiver for navigation and remote-sensing," in *Proc. 5th ESA Workshop Satell. Navigat. Technol. Eur. Workshop GNSS Signals Signal Process.*, Dec. 2010, pp. 1–7.
- [9] National Geospatial-Intelligence Agency (NGA), "Department of defense world geodetic system 1984, its definition and relationships with local geodetic systems," Tech. Rep. NGA.STND.0036_1.0.0_WGS84, vol. 1.0.0, Jul. 2014.
- [10] B. J. Southwell and A. G. Dempster, "The pseudo monostatic point for GNSS-R," in *Proc. IEEE Int. Geosci. Remote Sens. Symp.*, Jul. 2019, pp. 8729–8732.
- [11] W. Bosch and R. Savcenko, "On estimating the dynamic ocean topography - a profile approach," in *Gravity, Geoid and Earth Observation*, vol. 135, S. P. Mertikas, Ed., IAG Symposia, Springer, 2010. [Online]. Available: <https://help.veripos.com/hc/en-gb/articles/360002900511-Tides-What-is-the-relation-between-MSS-MSL-and-Geoid>
- [12] W. Fraczek, "Mean sea level, GPS, and the geoid," 2003. [Online]. Available: <https://www.esri.com/news/arcuser/0703/geoid2of3.html>. Accessed on: Jun. 6, 2020.
- [13] C. Ruf *et al.*, "A new paradigm in earth environmental monitoring with the CYGNSS small satellite constellation," *Sci. Rep.*, vol. 8, Jun. 2018, Art. no. 8782.
- [14] P. Jales, "Spaceborne receiver design for scatterometric GNSS reflectometry," Ph.D. dissertation, Univ. Surrey, Guildford, U.K., 2012.
- [15] *Copernicus Open Access Hub*, European Space Agency (ESA), Paris, France. Accessed: Jun. 6, 2020. [Online]. Available: <https://scihub.copernicus.eu/dhus/#/home>
- [16] A. W. Doerry and B. Brock, "Radar cross section of triangular trihedral reflector with extended bottom plate," Sandia National Laboratories, Albuquerque, NM, USA, Tech. Rep. SAND2009-2993, Jun. 2009.
- [17] G. Ruffini, "The GNSS-OPPCAT project and related work at the IECC," 1999. [Online]. Available: http://www.iecc.cat/hosted/oppscat/KNMI_slides/node21.html. Accessed: Jun. 6, 2020.
- [18] A. G. Voronovich and V. U. Zavorotny, "Bistatic radar equation for signals of opportunity revisited," *IEEE Trans. Geosci. Remote Sens.*, vol. 56, no. 4, pp. 1959–1968, Apr. 2018.
- [19] J. Maslanik and J. Stroeve, "Near-real-time DMSP SSMIS daily polar gridded sea ice concentrations, version 1," 1999, Updated daily, Subset Jul. 24, 2016, Boulder, CO, USA, 2019. [Online]. Available: <https://doi.org/10.5067/U8C09DWVX9LM>. Accessed on: Jun. 6, 2020.



Lucinda S. King (Student Member, IEEE) received the bachelor's degree in experimental and theoretical physics from the University of Cambridge, Cambridge, U.K., in 2013. She is currently working toward the Ph.D. degree in electrical and electronic engineering with the University of Surrey, Guildford, U.K., where her research focuses on the use of global navigation satellite system (GNSS) reflectometry for monitoring land parameters and the use of new GNSS signals.

From 2015 to 2018, she worked as a Space Systems Engineer with Airbus Defence and Space on a variety of projects related to GNSS, including the Galileo ground control segment, software receiver development, and R&D.



Martin Unwin worked toward the Ph.D. degree in spaceborne GPS with the University of Surrey, Guildford, U.K., from 1991 to 1995.

He initiated and led the GPS team in Surrey Satellite Technology Ltd. (SSTL), Guildford, U.K., designing the SGR-20 space GPS receiver which flew on UoSAT-12 and Proba-1. The GPS team succeeded in demonstrating autonomous orbit control, attitude determination in orbit, operation of GPS above the GPS constellation, and the development of GPS reflectometry instruments on UK-DMC, TDS-1, and

CYGNSS satellites. He had involvement in GIOVE-A and Galileo FOC projects from the beginning. He is currently a Principal Engineer with SSTL and is working on the development of newer generation receivers for remote sensing.



Jonathan Rawlinson received the M.Eng. degree in electrical and electronic engineering from Imperial College London, London, U.K., in 2018.

From 2012 to 2018, Jonathan worked as a Student RF Engineer with Defence Science and Technology Laboratory (DSTL) in a signals processing department. Jonathan is currently working as a GNSS Engineer in the RF & GNSS Team with Surrey Satellite Technology Ltd. (SSTL), Guildford, U.K., where he is focused on a diverse range of topics including developing novel GNSS+R algorithms, next generation

global navigation satellite system (GNSS) receiver development and GNSS receiver verification.



Raffaella Guida (Member, IEEE) received the Laurea degree (cum laude) in telecommunications engineering and the Ph.D. degree in electronic and telecommunications engineering from the University of Naples Federico II, Naples, Italy, in 2003 and 2007, respectively.

She held research positions with the University of Naples and the Technische Universität München and in 2008 joined the Surrey Space Centre (SSC), University of Surrey, Guildford, U.K., as a Lecturer of Satellite Remote Sensing. She is currently Head of the

Remote Sensing Applications research group and Director of the Postgraduate Research Programme in SSC. Her main research interests include electromagnetics and microwave remote sensing, simulation and modeling of Synthetic Aperture Radar (SAR) signals, new mission concepts and applications, satellite data fusion and interoperability.

Dr. Guida was one of the recipients of the IEEE J-STARS Best Paper Award 2013.



Craig Underwood (Member, IEEE) received the B.Sc. degree in physics with computer science from the University of York, York, U.K., in 1982, and the Ph.D. degree from the University of Surrey, Guildford, U.K., in 1996, with his work on the effects on the ionizing radiation on space electronics.

He has over 33 years experience in space systems engineering and has worked on numerous small satellite missions, specializing in sensors and instrumentation for radiation detection, optical, and radar remote sensing. He is currently Emeritus Professor

of Spacecraft Engineering with the Surrey Space Centre, University of Surrey, Guildford, U.K. He is the Author or Co-Author of some 200 scientific papers and still teaches modules on the Spacecraft Engineering degrees with the University of Surrey in his retirement.